OPEN

MagnetOs, Vitoss, and Novabone in a Multi-endpoint Study of Posterolateral Fusion

A True Fusion or Not?

Lukas A. van Dijk, MSc,*† Florence Barrère-de Groot, PhD,*
Antoine J.W.P. Rosenberg, MD, PhD,† Matthew Pelletier, PhD,‡ Chris Christou, PhD,‡
Joost D. de Bruijn, PhD,*§ and William R. Walsh, PhD‡

Study Design: This study was a multi-endpoint analysis of bone graft substitutes implanted as a standalone graft in a clinically relevant *Ovine* model of instrumented posterolateral spinal fusion (PLF).

Objective: The objective of this study was to obtain high-quality evidence on the efficacy of commercial bone graft substitutes compared with autograft in instrumented PLF using a state-of-the-art model with a complete range of assessment techniques.

Summary of Background Data: Preclinical and clinical data on the quality of spinal fusions obtained with bone graft substitutes are often limited. Calcium phosphates with submicron topography have shown promising results in PLF, as these are able to induce bone formation in tissues distant from the host bone, which facilitates bony union.

Methods: Nine female, skeletally mature sheep (4–5 y) underwent posterior pedicle screw/rods instrumented PLF at L2–L3 and L4–L5 using the following bone graft materials as a standalone graft per spinal segment: (1) biphasic calcium phosphate with submicron topography ($BCP_{<\mu m}$), (2) 45S5 Bioglass (BG), and (3) collagen-β-tricalcium phosphate with a 45S5 Bioglass adjunct (TCP/BG). Autograft bone (AB) was used as a positive control treatment. Twelve weeks after implantation, the spinal segments were evaluated by fusion assessment (manual palpation, x-ray, micro-computed tomography, and histology), fusion mass volume quantification (micro-computed tomography), range of motion (ROM) testing, histologic evaluation, and histomorphometry.

Results: Fusion assessment revealed equivalence between AB and $BCP_{<\mu m}$ by all fusion assessment methods, whereas BG and TCP/BG led to significantly inferior results. Fusion mass volume was highest for $BCP_{<\mu m}$, followed by AB, BG, and TCP/BG. ROM testing determined equivalence for spinal levels treated with AB and $BCP_{<\mu m}$, while BG and TCP/BG exhibited higher ROM. Histologic evaluation revealed substantial bone formation in the inter-transverse regions for AB and $BCP_{<\mu m}$, whereas BG and TCP/BG grafts contained fibrous tissue and minimal bone formation. Histologic observations were supported by the histomorphometry data.

Conclusions: This study reveals clear differences in efficacy between commercially available bone graft substitutes, emphasizing the importance of clinically relevant animal models with multi-endpoint analyses for the evaluation of bone graft materials. The results corroborate the efficacy of calcium phosphate with submicron topography, as this was the only material that showed equivalent performance to autograft in achieving spinal fusion.

Key Words: synthetic bone grafts, posterolateral fusion, preclinical model

(Clin Spine Surg 2020;33:E276–E287)

Spinal fusion procedures involve the use of bone grafts to mechanically and biologically conjoin ≥2 consecutive spinal segments. Posterolateral spinal fusion (PLF) is one of the more challenging bone grafting indications performed clinically, because it requires the formation of a large, consolidated bone mass through the paraspinous soft tissues with limited host bone contact. To avoid adverse effects related to the harvesting of iliac crest–derived bone graft,[1] synthetic bone graft materials are used as extenders or substitutes of autograft bone (AB). Numerous synthetic bone grafts are available on the market, of which many are based on calcium phosphate and bioactive glass.[2,3] Calcium phosphate materials are suitable bone graft materials due to their similar composition and structure to mineralized inorganic bone matrix, which

facilitates excellent osteoconductive and bone-bonding properties.[4] Besides this, specific surface characteristics of calcium phosphates have been shown to strongly affect bone regeneration in vivo. Submicron size and morphology of calcium phosphate surface features have been linked to an ability to induce bone formation in tissues distant from host bone without the addition of stem cells or growth factors, resulting in enhanced performance in orthotopic sites.[5–9] Bioactive glasses have been shown to release ionic dissolution products that can stimulate the activity of osteogenic cells in vitro,[10–12] termed osteostimulation. Bioactive glasses have also been shown to elicit deposition of a crystalline calcium phosphate surface layer in simulated body fluid,[13,14] which has been related to osteoconduction and strong bone-bonding in vivo.[15,16] Although different types of bioactive glass have been studied in recent years, 45S5 bioactive glass (ie, Bioglass) developed by Hench and colleagues has been most well-known as a bone graft substitute material.[3]

The selection of the most appropriate bone graft for PLF may be challenging for surgeons, because preclinical studies on these materials have mostly been performed in nonclinically relevant models. Few studies have compared materials from different classes of synthetic bone grafts (eg, calcium phosphate, Bioglass) in spinal fusion models in vivo. However, side-by-side comparison of such materials in well-designed, clinically relevant animal models could provide valuable insights that could aid surgeons in the selection of treatment options for spinal surgery.

Recently, this research team demonstrated equivalent performance between a calcium phosphate with submicron topography and the gold standard, autograft, in clinically relevant animal models of PLF.[17,18] One of these studies involved a challenging *Ovine* model of instrumented PLF with implantation as a standalone bone graft. In the current work, this *Ovine* PLF model was again utilized to compare 3 commercially available bone grafts based on calcium phosphate and 45S5 Bioglass. The groups included were (1) a putty formulation of BCP (biphasic calcium phosphate) with submicron surface topography, previously shown to have equivalent performance to autograft in this model,[17,18] (2) a putty formulation of 45S5 bioactive glass, (3) a collagen-β-tricalcium phosphate (βTCP) composite with a 45S5 bioactive glass adjunct. AB was included as the "gold standard" reference treatment. Twelve weeks following implantation, the treated segments were evaluated by a range of assessment methods, including fusion assessment [manual palpation, x-ray, micro-computed tomography (CT), and histology], biomechanical range of motion (ROM) testing, fusion mass volume quantification (micro-CT), histologic evaluation of tissue responses, and histomorphometry of bone tissue and residual graft material.

METHODS

Materials

Three commercially available bone grafts were examined in this study. The submicron structured biphasic calcium phosphate bone graft was provided in a putty formulation (BCP$_{<\mu m}$; MagnetOs Putty; Kuros Biosciences BV, The Netherlands). This formulation contained 1–2 mm calcium phosphate granules with a submicron surface topography[6] and a phase composition of 65%–75% βTCP and 25%–35% hydroxyapatite, embedded in a fast-resorbing polymer carrier. The polymer carrier consisted of polyethylene glycol and L-lactide monomer and occupied the granule pores and intergranular space. MagnetOs Putty is currently not labeled for use as standalone bone graft in spinal fusion surgery in the United States.

The bioactive glass-based bone graft was a putty formulation (BG; Novabone Putty; Novabone Products LLC) and consisted of ±70 vol/vol% bioactive glass (45S5) particles of 32–710 μm in a water-soluble carrier of polyethylene glycol and glycerin. 45S5 bioactive glass is composed of ±45% silica (SiO_2), 24.5% calcium oxide (CaO), 24.5% sodium oxide (Na_2O), and 6% phosphorous pentoxide (P_2O_5) (wt%).[15]

The collagen-βTCP composite with 45S5 Bioglass (TCP/BG; Vitoss BA2X Foam pack, Orthovita Inc.) was comprised of a bovine type I collagen carrier containing βTCP particles (≥95%–100% βTCP) of 1–4 mm, with a separate vial of 1.5 g 45S5 bioactive glass particles of 90–150 μm. The implant was prepared according to the instructions for use. In short, the bioactive glass particles were loaded onto the collagen-βTCP composite, after which physiological saline was added, and the composite was thoroughly mixed. The final composition of the graft was ±55% βTCP, 27% 45S5, and 18% collagen (wt%).

Animal Study

A previously described *Ovine* model of 2-level instrumented PLF was used in this study.[18] Nine female, skeletally mature sheep (*Ovis Aries*, Border Leicester Merino Cross, 4–5 y, 80–90 kg) were used at the University of New South Wales, Australia, following approval from the local Animal Care and Ethics Committee (ACEC). The animals were randomly allocated treatments at levels L2–L3 and L4–L5 according to a randomization scheme, with n = 6 for AB, n = 6 for BCP$_{<\mu m}$, n = 3 for BG, and n = 3 for TCP/BG. After the administration of appropriate antibiotics, analgesics, and anesthetics, surgery was performed, as previously described.[18] In brief, the animal was positioned in sternal recumbency and draped using sterile technique. The correct levels were identified and marked preoperatively using fluoroscopy. A skin incision was made in the dorsal midline, after which facet joints and transverse processes (TPs) for the relevant levels were exposed and decorticated. The 2 operative levels (L2–L3 and L4–L5) were instrumented bilaterally with polyaxial pedicle screws (Ø 5.5×25 mm) and solid titanium rods (Ø 5.5 mm). Thereafter, 2 single-level posterolateral arthrodeses were performed at the exposed levels. For each graft material, 10 cm³ of material was placed into both posterolateral gutters (20 cm³ total per level) at the appropriate level in direct apposition with the decorticated TPs, spanning the intertransverse process

space. Corticancellous autograft was obtained from the bilateral *Os Ilium*s using rongeurs, after removal of the cortex. Autograft was reduced to 2–5 mm bone chips that were mixed to obtain a 1:1 ratio of both donor sites. The surgical sites were closed in layers. Postoperatively, the animals were monitored and received proper postoperative care, antibiotics, and analgesics. At 12 weeks' follow-up, animals were anesthetized and euthanized by lethal injection of Lethobarb (325 mg/2 kg intravenously). The lumbar spines were excised and harvested for endpoint analyses.

Manual Palpation

Directly after harvesting of the spines and removal of the pedicle rods, 2 trained observers assessed fusion rigidity of the treated spinal levels in a blinded manner by manual palpation, as previously described.[19] All levels were graded as fused (rigid, low mobility) or not fused (not rigid, high mobility) in lateral bending (LB) and flexion-extension (FE), with an untreated level used as a relative comparison.

Radiography

Faxitron

Harvested spines were radiographed in the posteroanterior plane using a Faxitron (Faxitron Bioptics LLC, Tucson, AZ) and digital plates (Agfa CR MD 4.0 cassette; Agfa, Germany). An Agfa Digital Developer and workstation was used to process the digital images (Agfa CR 75.0 Digitizer Musica; Agfa). The radiographic status of the spinal arthrodesis was evaluated by 2 experienced observers in a blinded manner on anteroposterior radiographs using the Lenke 4-point grading scale[20] (Table 1).

Micro-CT

Micro-CT was performed on the spines using an Inveon Scanner (Siemens Medical Solutions USA Inc., Knoxville, TN). Scans were made with a slice thickness of 53 µm and were stored in DICOM format. Three-dimensional reconstructions were generated from the scans. Status of the spinal arthrodesis was evaluated by 2 experienced observers in a blinded manner in 3 orthogonal planes (ie, axial, sagittal, coronal) and anterior and posterior 3-dimensional reconstructions. As for the radiographs, the Lenke 4-point grading scale was used to grade fusion status.

Quantification of Fusion Mass Volume

Fusion mass volume quantification was performed on TIFF stacks generated from the DICOM scans of the treated spinal levels using dedicated image computing software (3D Slicer 4.10[21]). This was achieved by performing manual, intensity-based selection of the separate left and right fusion masses on interspersed axial slices (53 µm) throughout the micro-CT files, taking care to exclude the host vertebrae and TPs. Subsequently, interpolation of boundaries between adjacent scan layers was performed using a contour interpolation algorithm,[22] resulting in segmentations of the fusion mass. The total volume of each fusion mass in cm^3 was derived from the number of voxels in each segmentation, including both (new) mineralized bone and residual graft material.

Biomechanical Analysis

Nondestructive biomechanical ROM testing was performed to obtain a multidirectional flexibility profile of the treated spinal levels. After removal of the pedicle rods, each of the spinal levels was mounted onto a 6-axis sim-VITRO robotic musculoskeletal simulator (Simulation Solutions Ltd, Stockport, UK and Cleveland Clinic Biorobotics Lab, Cleveland, OH). A ±7.5 Nm pure moment was applied to the spinal levels in LB, FE, and axial rotation (AR). Each loading profile was repeated 3 times, and a mean value for LB, FE, and AR was recorded in the ROM degrees.

Histology and Histomorphometry

Following mechanical testing, spines were fixed at room temperature in 10% formalin in 0.145 M phosphate-buffered saline under gentle rotation for at least 96 hours. Subsequently, specimens were processed for polymethylmethacrylate embedding. A Leica SP1600 saw microtome was used to cut sections in the sagittal plane from the region between TPs lateral of the spine at both sides. From each side, a minimum of 3 sections separated by 300 µm was obtained. A histologic staining of methylene blue (Sigma; 1% in 0.1 M borax buffer, pH 8.5) and basic fuchsin (Sigma; 0.3% in demi water) was performed to visualize bone tissue (bone matrix: pink, fibrous tissues: blue). Sections were examined under a Leica microscope (Eclipse 50i; Nikon) and were scanned with a slide scanner (DiMage scan 5400 Elite II; Konica Minolta, Tokyo, Japan) to obtain low-magnification overviews.

Histologic Evaluation and Fusion Assessment

Histologic evaluation included qualitative assessment of the tissue response, including evidence of inflammation, evidence of graft resorption, new bone formation, and bone marrow space development. Low-magnification overviews of each section were used for fusion assessment and histomorphometry. Fusion assess-

TABLE 1. Fusion Grading Scale for X-Ray and Micro-Computed Tomography Assessment Based on the Lenke Classification[20]

Grade	Definition
A	Bilateral robust bridging fusion masses (definitely solid)
B	Unilateral robust bridging fusion mass and contralateral thin fusion mass (probably solid)
C	Unilateral thin bridging fusion mass and probable pseudarthrosis on the contralateral aspect (probably not solid)
D	Bilateral thin fusion masses with obvious pseudarthrosis or bone graft resorption (definitely not solid)

TABLE 2. Outcomes of Fusion Assessment Per Evaluation Method

Methods	AB	BCP$_{<\mu m}$	BG	TCP/BG	Significance (P)*
Manual palpation	6/6	6/6	1/3	1/3	0.013
X-ray	A: 4/6	A: 5/6	B: 2/3	C: 1/3	0.008
	B: 2/6	B: 1/6	D: 1/3	D: 2/3	
Micro-CT	A: 3/6	A: 5/6	B: 2/3	C: 1/3	0.010
	B: 3/6	B: 1/6	D: 1/3	D: 2/3	
Histology	9/12	10/12	0/6	0/6	< 0.001

*Fisher-Freeman-Halton exact test.
AB indicates autograft bone; BCP$_{<\mu m}$, biphasic calcium phosphate with submicron topography; BG, Bioglass; CT, computed tomography; TCP, tricalcium phosphate.

ment by histology was performed by 2 trained observers in a blinded manner on 3 sections from each lateral side of the treated spinal level, resulting in 2 scores per level. Each section was scored as histologically fused if a continuous bridge of bone tissue was observed between the TPs of L2–L3 or L4–L5, thus connecting the adjacent spinal levels. When at least 1 of the 3 sections was scored as fused, the sample was considered "fused" on that side of the spine. If no fusion was determined in any of the 3 slides, the sections were digitally stacked and reevaluated for fusion.

Histomorphometry

Histomorphometry of the fusion mass was performed on 3 sections from each side of the treated spinal level. Pixels representing bone (B) and remaining implant material (M) in a region of interest (ROI) were pseudo-colored using image editing software (Adobe Photoshop 5.0). Next, the number of pixels for B, M, and ROI was recorded, and the area percentage of bone in the available space was calculated by the following formula: B/(ROI−M)× 100%. In addition, the area percentage of remaining implant material was calculated by the following formula: M/ROI×100%.

Statistical Analysis

Statistical analysis of data was performed using dedicated software tools (GraphPad Prism, San Diego, CA; SPSS Inc., Chicago, IL). Fusion grading data from manual palpation, x-ray, micro-CT, and histology were analyzed by the Fisher-Freeman-Halton exact test. Data from micro-CT volume quantification, biomechanical ROM testing, and histomorphometry were analyzed by analysis of variance followed by Tukey honest significant difference test for post hoc analysis. Normal distribution of data was assessed by the Shapiro-Wilk normality test. For all statistical tests, a significance level of *P*-value <0.05 was utilized.

RESULTS

Surgery

All surgeries and study procedures proceeded as planned. All graft materials handled well, as they were moldable and easy to implant into the posterolateral gutters. No adverse events occurred in any animal during surgery and the 12-week follow-up period.

Manual Palpation

Results of fusion assessment by manual palpation are presented in Table 2. Successful arthrodesis was confirmed in all levels treated with AB, with 100% of specimens graded as rigid in both LB and FE. Results varied between treatment groups. Although BCP$_{<\mu m}$ showed a similar fusion rate to AB with all specimens scored as rigid, both bone grafts (BG and TCP/BG) containing bioactive glass were graded as rigid in only 1 of 3 treated levels. All fusion grades by manual palpation were coherent between reviewers and between the different modes LB and FE. The difference between groups was confirmed by statistical analysis.

Radiographic Evaluation and Fusion Assessment

Faxitron radiographs (Fig. 1) were evaluated for evidence of bone formation and residual graft material in the posterolateral regions in between TPs of L2–L3 and L4–L5. In the AB group (Fig. 1A), a consolidated mass of mineralized bone was observed in the bilateral intertransverse process regions. Individual autogenous bone particles could not be discriminated. In the BCP$_{<\mu m}$ group (Fig. 1B), a large, radiopaque fusion mass was evident in the region between the bilateral TPs. Although individual BCP$_{<\mu m}$ particles could still be discriminated, the grafts had consolidated into a dense, continuous fusion mass between the TPs. At levels treated with BG (Fig. 1C), thin masses of radiopaque material, which were of variable intensity and continuity, were observed between TPs. In the TCP/BG group (Fig. 1D), there was a significant lack of radiopaque substance in the intertransverse regions of all treated levels. The TCP/BG grafts had a low radiopacity with a granular appearance and did not form a consolidated mass at the treated levels.

On micro-CT reconstructions (Fig. 2), a bony fusion mass forming a bridge between L2–L3 or L4–L5, was commonly observed in the AB group (Fig. 2A). In many cases, the fusion masses were well-developed, showing a smooth, continuous bone mass with a de novo cortex. Occasionally, fusion masses were not yet completely consolidated and matured, as an outer cortex had not yet developed, and autograft chips could be distinguished in the developing bone mass. The BCP$_{<\mu m}$ grafts (Fig. 2B) formed uniform, solid, and continuous fusion bridges between the TPs. The center of the BCP$_{<\mu m}$ grafts was compact, and individual BCP particles could be hardly
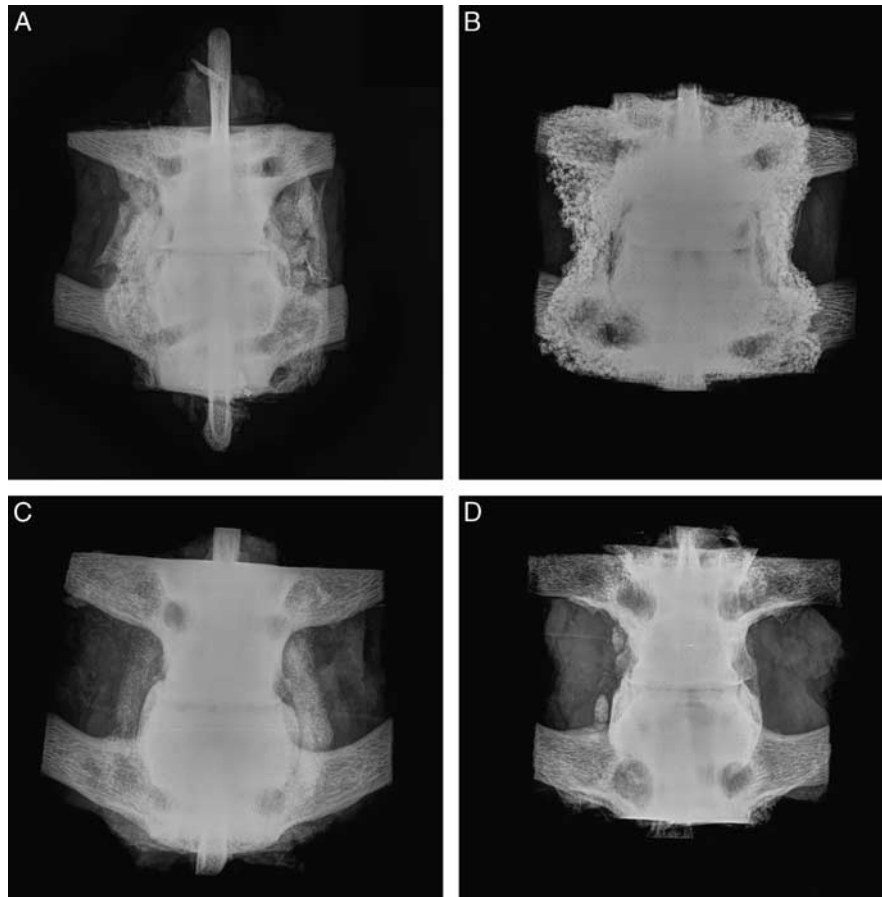
FIGURE 1. Representative examples of faxitron radiographs of the spinal levels treated with AB (A), $BCP_{<\mu m}$ (B), BG (C), and TCP/BG (D), after removal of instrumentation. AB indicates autograft bone; $BCP_{<\mu m}$, biphasic calcium phosphate with submicron topography; BG, Bioglass; TCP, tricalcium phosphate.

distinguished on axial, sagittal, and transversal slices, indicating bone formation between the granules. New bone growth into the calcium phosphate grafts could be observed in the regions near the host bone.

The spinal levels treated with BG (Fig. 2C) presented thin, underdeveloped fusion masses versus AB and $BCP_{<\mu m}$, as observed by micro-CT. The radiopaque mass, in the region between TPs (if present), had a fine, granular appearance with localized, dense regions in the center or in apposition with TPs. A continuous mass between TPs was lacking, and Bioglass granules were few and dispersed. None of the treated levels presented a consolidated fusion mass between TPs with TCP/BG (Fig. 2D). A small amount of dispersed, granular material was occasionally observed in the intertransverse regions. In some cases, regions of minor osteoconductive bone growth were observed near the host bone.

Results of fusion grading on radiographs and micro-CT according to the Lenke scale are presented in Table 2. Both AB and $BCP_{<\mu m}$ obtained high fusion scores, with either unilateral or bilateral robust bone bridging in all treated levels. Radiographic fusion scores were lower in the other groups, while the BG group obtained more favorable grades than TCP/BG. The differences in radiographic fusion grades reached statistical significance, although no between-group comparisons were analyzed.

Fusion Mass Volume

Micro-CT quantification (Fig. 2E) revealed that the levels treated with AB had an average unilateral, mineralized fusion mass volume of $5.70 \pm 1.59 \, cm^3$. The volume in the $BCP_{<\mu m}$ group was significantly higher at $9.60 \pm 0.45 \, cm^3$. Volumes were significantly lower in BG and TCP/BG, at $\sim 3 \, cm^3$. Statistical significance was reached for all group comparisons, except for BG versus TCP/BG.

Biomechanical Testing

Functional treatment efficacy was quantified by use of biomechanical ROM testing (Fig. 3). The $BCP_{<\mu m}$ group revealed an equivalent ROM to AB in all modes, while ROM for levels treated with BG and TCP/BG was evidently higher in LB and FE. Statistical analysis revealed equivalence between AB and $BCP_{<\mu m}$ in all modes, while ROM in these groups was significantly lower in LB and FE compared with BG and significantly lower in FE compared
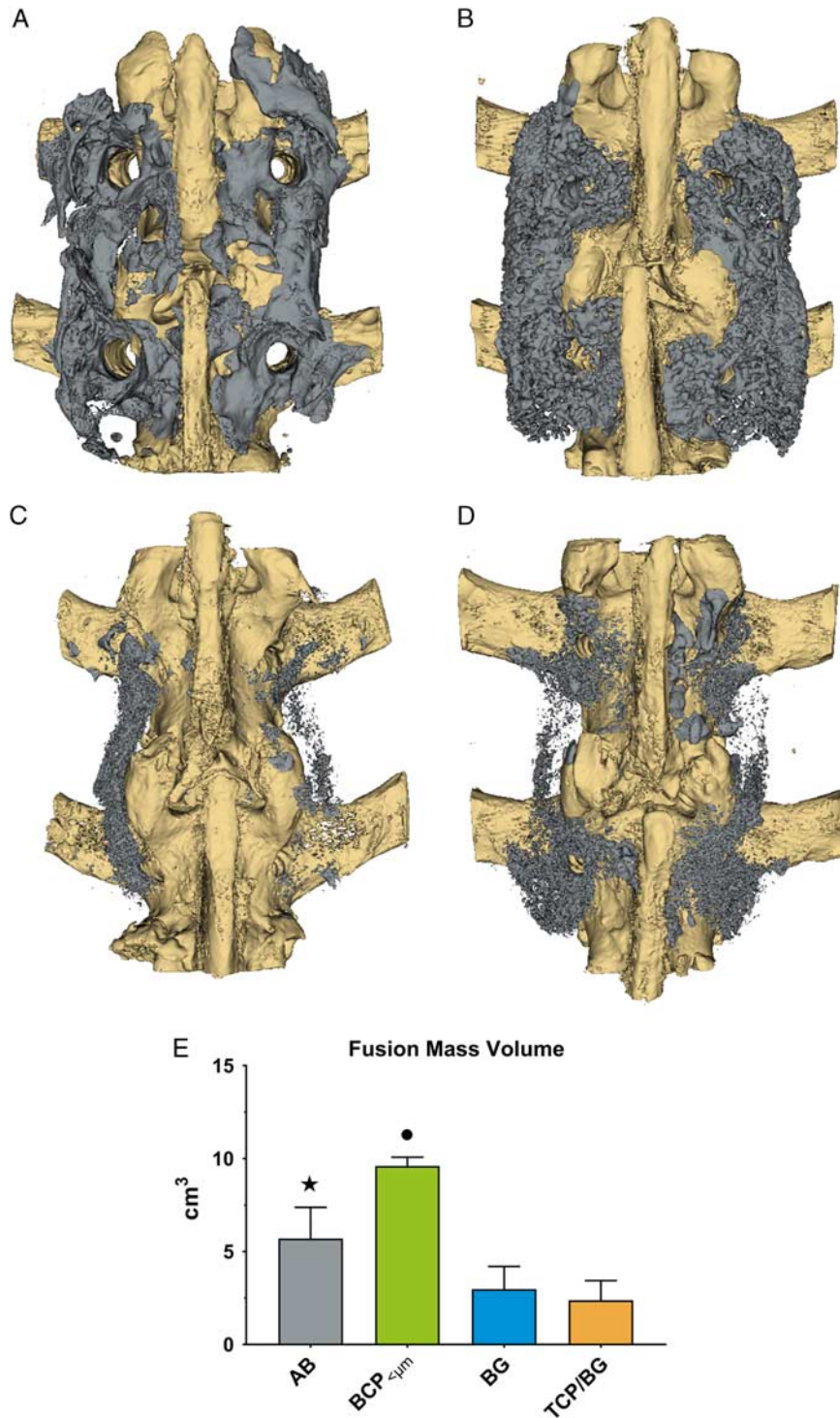
FIGURE 2. Representative examples of 3-dimensional micro-computed tomography reconstructions (A–D) of spinal levels treated, AB (A), $BCP_{<\mu m}$ (B), BG (C), and TCP/BG (D). The host spinal bone (off-white) and fusion mass (gray) including (new) bone and residual implant material are shown as individual segmentations. For each treatment group, unilateral fusion mass volume (bone+ graft material) was determined by performing voxel-based quantification (E). Data shown as mean and SD. ●, significantly different from AB, BG, and TCP/BG ($P < 0.001$). ★, significantly different from $BCP_{<\mu m}$, BG, and TCP/BG ($P < 0.001$). AB indicates autograft bone; $BCP_{<\mu m}$, biphasic calcium phosphate with submicron topography; BG, Bioglass; TCP, tricalcium phosphate.

FIGURE 3. Diagrams of nondestructive biomechanical range of motion testing results, as performed in lateral bending (A), flexion-extension (B), and axial rotation (C). Data are presented as range of motion degrees in mean and SD. ★, significantly different from AB and BCP$_{<\mu m}$ ($P < 0.005$). •, significantly different from AB and BCP$_{<\mu m}$ ($P < 0.05$). ▪, significantly different from AB and BCP$_{<\mu m}$ ($P < 0.005$). AB indicates autograft bone; BCP$_{<\mu m}$, biphasic calcium phosphate with submicron topography; BG, Bioglass; TCP, tricalcium phosphate.

with TCP/BG. No significant difference in AR ROM was determined between all treatments.

Histologic Evaluation and Fusion Assessment

Histology of the spinal levels treated with AB (Fig. 4A) revealed the presence of abundant new and remodeling bone tissue in the intertransverse process space. The implanted AB particles had been remodeled into uniform bone mass in the intertransverse process space.

In BCP$_{<\mu m}$ specimens (Figs. 4B, 5A–D), a large area consisting of calcium phosphate granules integrated in trabecular bone was observed throughout the implant sites (Fig. 4B). Bone was of mature, lamellar morphology including new bone marrow spaces (Figs. 5A–C) and evidence of a pseudocortex in some specimens (Fig. 5D). The bone matrix was in direct apposition with the BCP$_{<\mu m}$ material. Typical bone cells, including osteoblasts lining regions of new bone formation, osteoclasts, and osteocytes were observed throughout the specimens (Fig. 5C) Multinucleated cells were observed resorbing the calcium phosphate material on granule surfaces not covered by bone (Fig. 5C).

Histology of the BG specimens (Figs. 4C, 5H–K) presented as fibrous tissue with dispersed Bioglass particles and absence of bone tissue throughout the implant site

(Fig. 4C). Residual Bioglass particles were contained in fibrous tissue and commonly contained cracks, sometimes having a hollow center, or were fragmented (Fig. 5H). Occasional osteoconductive bone formation was observed in the vicinity of host TPs (Fig. 5E). However, sometimes, no osteoconductive bone formation was observed even when Bioglass was in direct apposition with the host bone (Fig. 5G). In 5 of 6 specimens, a foreign body reaction was observed around Bioglass particles throughout the implant sites, characterized by encapsulation by granulatomous inflammatory tissue with presence of lymphocytes and foreign body giant cells (Figs. 5I–K). Moreover, 3 of 6 specimens contained dense regions of Bioglass of variable dimensions, which upon further inspection revealed to be areas of severely fragmented material and evidence of foreign body reaction (Fig. 5J).

For TCP/BG (Figs. 4D, 5L–P), most sections had to be obtained from regions very medial to the spinal body, as graft material or bone in the regions between TPs was largely absent (Fig. 4D). The implantation sites contained fibrous tissue with sparse calcium phosphate particles, which were commonly in the process of disintegration due to cell-mediated resorption (Figs. 5N–O). The Bioglass particles were very small and could only be observed by high magnification, with a similar appearance to those

FIGURE 4. Representative, low-magnification micrographs of sagittal histologic sections (methylene blue/basic fuchsin) taken from the intertransverse process regions of spinal levels treated with AB (A), $BCP_{<\mu m}$ (B), BG (C), and TCP/BG (D). Bone matrix is shown in pink, soft tissues in blue, residual calcium phosphate material in black, and Bioglass particles are translucent. The low-magnification micrographs were graded for fusion, evident from a continuous bone bridge between adjacent transverse processes. AB indicates autograft bone; $BCP_{<\mu m}$, biphasic calcium phosphate with submicron topography; BG, Bioglass; TCP, tricalcium phosphate.

observed in the BG group (Figs. 5L–P). An inflammatory reaction around the Bioglass particles was generally not observed. Newly formed bone tissue was absent in the central region of the implants, although some specimens exhibited new bone formation in the vicinity of TPs. Calcium phosphate and Bioglass particles were occasionally observed being integrated in the bone matrix (Figs. 5L–M). One specimen presented a region with graft material enclosed by granulatomous tissue that contained high numbers of lymphocytes and resorbing multinucleated giant cells, indicating a foreign body granuloma (Fig. 5P).

Results of fusion assessment by histology are presented in Table 2. Histologic fusion scores in the AB and $BCP_{<\mu m}$ groups were significantly higher than in the BG and TCP/BG groups. For levels treated with AB, the positive control, fusion was reported in 9 of 12 samples, corresponding to a fusion rate of 75%. In the $BCP_{<\mu m}$ group, 10 of 12 samples were scored as fused, which translates to a fusion rate of 83%. For the BG and TCP/BG groups, a bony fusion between TPs was not reported in any of the specimens, thus corresponding to a fusion rate of 0%. Statistical analysis revealed that the differences in histologic fusion rate were statistically significant ($P < 0.05$).

Histomorphometry

As determined by histomorphometry (Fig. 6), the fusion masses of levels treated with AB and $BCP_{<\mu m}$ contained a substantially higher percentage of bone, as compared with the BG and TCP/BG groups (Fig. 6A). Bone proportions were similar for AB and $BCP_{<\mu m}$, with over >40% of bone in the available space in both groups. This percentage was significantly lower for the other groups,

the lowest being BG, followed by TCP/BG. Statistical analysis confirmed equivalence for AB versus $BCP_{<\mu m}$ and BG versus TCP/BG, while all other comparisons were significantly different. Area percentage of remaining graft material (Fig. 6B) was highest for $BCP_{<\mu m}$ implants, followed by BG, with the TCP/BG graft having the lowest percentage. Statistical significance was reached for all group comparisons in material percentage.

DISCUSSION

The posterolateral spine environment is a challenging biological and biomechanical environment, as it provides limited host bone contact and significant exposure to soft tissues. Even with use of the "gold standard" of autograft, surgeons commonly deal with revision surgery rates of ±10%–20%.[23–26] Considering this, it is important that the selection of graft materials is based on preclinical evidence obtained in studies of high methodological quality, using clinically relevant animal models and multiple evaluation techniques. A large number of bone grafts are commercially available for clinical use, which makes selection of the most appropriate challenging for the surgeon community. Most reports on commercial graft materials in the literature are of preclinical studies performed in rabbits, and they involve the repair of small, cancellous bone defects with a high ratio of bone surface to defect volume.[27–33] Although critically sized, that is, they will not completely spontaneously heal without the use of a graft, such defects are less challenging than, and do not properly model, the posterolateral spine environment. This limits the extrapolation of results from these models to PLF indications. Moreover, many studies have been of poor
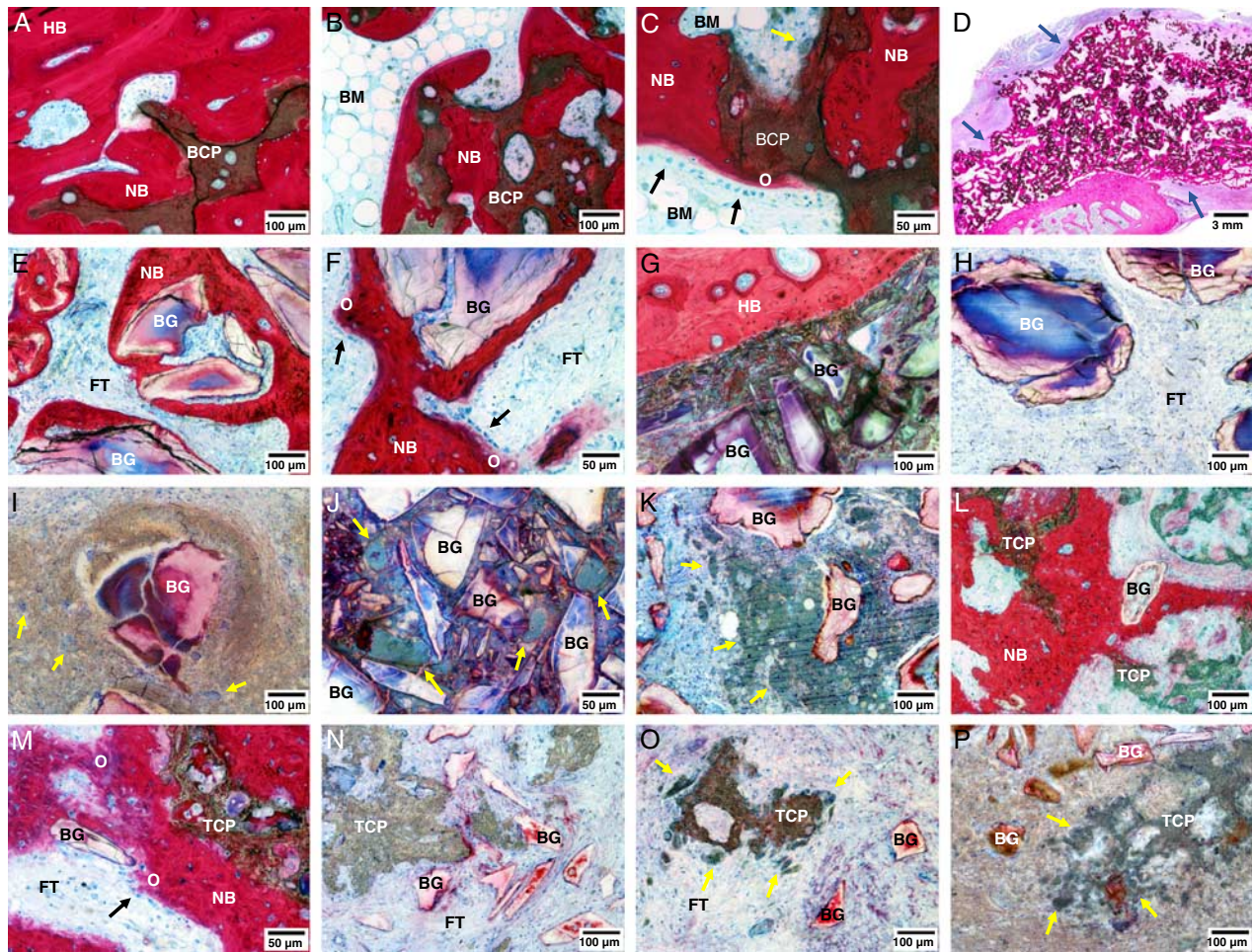
FIGURE 5. Representative micrographs from histologic sections of the spinal levels treated with BCP$_{<\mu m}$ (A–D), BG (E–K), and TCP/BG (L–P). Micrographs were obtained from regions near the host transverse process (A, E–G, L, M) and the intertransverse central region (B, C, H–K, N–P). A pseudocortex on the outside of the fusion mass was observed in specimens treated with BCP$_{<\mu m}$ (D—blue arrows). High-magnification images show cellular processes observed near the graft materials, including osteoblasts (C, F, M—black arrows) depositing osteoid and cell-mediated resorption of materials by multinucleated cells (C, O, P—yellow arrows). Inflammatory foreign body reaction was observed in BG and TCP/BG specimens, as evidenced by encapsulation of material (I), high numbers of lymphocytes (I, P) and foreign body giant cells (I–K, P—yellow arrows). BCP$_{<\mu m}$ indicates biphasic calcium phosphate with submicron topography; BG, Bioglass; BM, bone marrow; FT, fibrous tissue; HB, host bone; NB, new bone; O, osteoid; TCP, tricalcium phosphate.

methodological design, for example, no use of critical-sized defects, lack of proper positive and/or negative controls, and use of limited endpoints and assessment methods with low sensitivity.[27–29,34] Clinical reports for the use of synthetic bone grafts are limited in number and often of low methodological strength (ie, observational studies). Furthermore, outcomes can only be determined using techniques with low sensitivity and/or specificity, such as radiographic evaluation and patient-reported outcomes.

Of the available animal models of PLF, the instrumented *Ovine* PLF[35] model is among the most translational, as bone remodeling properties and spine biomechanics of sheep are similar to those of humans, and the model allows the use of relevant graft volumes and pedicle instrumentation.[36–39] For comparison, the Boden

rabbit PLF model,[19] which is used to obtain market approval for bone graft materials in the United States, is noninstrumented and differs in anatomy, biomechanics, and bone turnover rate from the clinical reality in humans.[40] Note, the current study used aged sheep (4–5 y old), which challenges the model due to age.[41]

With regard to assessment techniques used for fusion evaluation, it is important that a range of different methods is applied, as they may individually give limited information and vary in sensitivity. Classically, fusion assessment in preclinical models was performed by the less sensitive techniques of manual palpation and plain film radiography.[19] Recently, more sensitive techniques have been added, including micro-CT, histology, and biomechanical testing. For synthetic bone grafts, fusion evaluation by radiography (eg, x-ray, CT) may lead to an overestimation of fusion, as bone mineral and

FIGURE 6. Histomorphometry diagrams of bone (A) and residual material (B) performed on low-magnification micrographs of histologic sections. Data are presented as area%, in mean and SD. ★, significantly different from BG and TCP/BG ($P<0.001$). ●, significantly different from BG ($P<0.005$) and TCP/BG ($P<0.001$). ■, significantly different from BCP$_{<\mu m}$ ($P<0.005$) and TCP/BG ($P<0.001$). AB indicates autograft bone; BCP$_{<\mu m}$, biphasic calcium phosphate with submicron topography; BG, Bioglass; TCP, tricalcium phosphate.

radiopaque implant materials cannot easily be distinguished by these methods. Histology provides a unique insight and accurate representation of a fusion mass at the tissue and cell level, allowing investigators to differentiate between bone and graft material and to evaluate tissue and cellular responses. Last, biomechanical testing is an important quantitative method performed in conjunction with the other techniques to determine whether fusion outcomes also have a functional significance, that is, reduction of mobility between spinal segments. Here, a robotic musculoskeletal simulator was used to apply controlled loading regimens to the spinal segments.

Using this validated, multi-endpoint, clinically relevant, *Ovine* model of instrumented PLF, 3 commercially available bone grafts implanted as a standalone graft were compared against AB, the current gold standard for bone grafting. Of the evaluated synthetic bone grafts, BCP$_{<\mu m}$ was the only material that presented substantial, solid fusion masses between TPs that contained mature bone, resulting in similar fusion scores to AB by all assessment methods and equivalent biomechanical ROM. These outcomes were corroborated by all assessment techniques and were in line with previous results.[17,18] In contrast to BCP$_{<\mu m}$, spinal levels treated with BG and TCP/BG significantly underperformed to the positive control by all evaluation methods. Although by biomechanical testing no significant differences between treatments were determined in AR, it is recognized that flexibility testing in AR has a lower sensitivity than the other modes.[42,43]

These results confirm the limitations of fusion evaluation by radiographic techniques when synthetic bone graft materials are used in PLF. Although spinal levels treated with BG obtained a moderate fusion grade B of the Lenke scale in 2 of 3 specimens by both x-ray and micro-CT, histology revealed that all apparent fusion bridges did not contain any bone tissue. These results show that the option to use histology is a significant advantage of preclinical models over clinical investigation. Histology also allows the evaluation of local tissue reactions, as the materials resorb

and participate in the bone repair and remodeling process, which is not possible by other techniques.

Fusion mass volume quantification is a more novel method for evaluation of PLF outcomes that assists in further differentiation of radiographic endpoints. It should be noted that the use of micro-CT, which is not available clinically, provides a level of detail beyond traditional radiographs or clinical CT. The technique can provide meaningful information on graft volume stability, as too fast or too severe resorption of a graft may potentially result in atrophic pseudarthrosis.[44] Here, clear differences in fusion mass volumes were determined between groups. Although the same starting volume of 10 cc was implanted in each posterolateral gutter for all groups, the mineralized volume after 12 weeks was around 3 cm^3 for BG and TCP/BG grafts, whereas for BCP$_{<\mu m}$, it was just under 10 cm^3. Although the initial radiopaque volume of the grafts was not determined and the data represent the volume of both new bone and residual graft material, we may still assume that BG and TCP/BG have undergone substantial resorption after implantation. This notion was supported by histologic observations and histomorphometry results. The finding that spinal levels treated with AB had lower fusion mass volumes compared with BCP$_{<\mu m}$ may be potentially related to a lower initial radiopaque volume, but could also suggest resorption. Indeed, AB has been reported to undergo resorption and remodeling after implantation in the posterolateral spine, leading to a volume loss of up to $\pm 35\%$ during the first year.[45–47]

The above findings demonstrate a clear difference in the performance of commercially available synthetic bone grafts in instrumented PLF in sheep. Correlation of performance outcomes to specific bone graft factors is challenging due to the many physicochemical differences between the grafts that could affect bone regeneration potential, for example, composition, surface properties, carrier materials, particle size, and graft to carrier ratio. However, the submicron surface topography of BCP$_{<\mu m}$ seems to play a leading role in bone graft performance[48] and may explain its enhanced efficacy in this PLF model.

In recent years, research has consistently demonstrated that calcium phosphates with a submicron topography show enhanced performance to conventional calcium phosphates, following from their ability to induce bone formation in regions far from host bone or with minimal bone contact.[7–9,48] This property is particularly desirable for use in PLF, in which bone formation should occur in the paraspinous soft tissues with limited host bone surface contact. A suggested mechanism underlying the enhanced efficacy of calcium phosphates with submicron topography is the upregulation of anti-inflammatory M2 macrophages at the material surface, which have been associated with bone regeneration (R. Duan, Y. Zhang, L.A. van Dijk, D. Barbieri, J.J.J.P van den Beucken, H. Yuan, J.D. de Bruijn, 2019, unpublished data).[49–51]

Bone induction by the TCP component of the TCP/BG group has been evaluated in 2 previous studies.[48,52] Both studies demonstrated the absence of submicron topography correlated with the lack of ectopic bone induction, even in the presence of Bioglass.[52] Furthermore, the TCP component in TCP/BG reportedly consists of 100% phase pure βTCP and has a porosity of 78%.[52] A calcium phosphate with these properties is expected to have a high resorption rate, with potentially detrimental effects on bone healing.[53] This notion is in agreement with the findings of the current study and other works.[32,33,52,53]

The presence of 45S5 Bioglass in BG and TCP/BG grafts, resulting in enhanced osteoblast activity and osteogenic differentiation of stem cells in vitro,[10–12,54–56] did not promote spinal fusion in this 1 PLF model. To our knowledge, there is no literature on the use of Bioglass as a standalone graft in PLF models, and beneficial effects of osteostimulation have not been demonstrated in other in vivo models. We may, therefore, conclude that osteostimulative Bioglass, whether used alone or as an adjunct to calcium phosphate, has little biological relevance to use of bone graft materials in spinal fusion. Moreover, the inflammatory foreign body reaction observed around Bioglass particles, which has also been reported in other studies,[57–59] is presumably not beneficial for bone formation. However, foreign body reaction against Bioglass particles was not observed in TCP/BG, which contained a lower content of Bioglass than BG (25% vs. 100%), suggesting that only larger proportions of Bioglass may induce such reactions.

CONCLUSIONS

Using a challenging, clinically relevant, *Ovine* model of instrumented PLF, this study reveals clear differences in performance between commercially available bone graft materials implanted as a standalone graft, after evaluation by a full range of assessment techniques. The results demonstrated favorable outcomes with a putty formulation of BCP$_{<\mu m}$, which has a submicron topography, versus 2 other bone graft materials, being a putty formulation of 45S5 Bioglass and a collagen-βTCP with a 45S5 Bioglass adjunct. Through all outcomes, the BCP$_{<\mu m}$ reached equivalence to the positive control, autograft, in achieving functional spinal fusion, while the other 2 materials significantly underperformed, showing an inability to form a solid, bony fusion between the spinal segments during the 12-week follow-up period. These results corroborate previous findings on the efficacy of BCP$_{<\mu m}$ with submicron topography in spinal PLF models, following from its ability to promote bone formation in soft tissues distant from host bone. These findings emphasize the importance of side-by-side comparison of commercial bone graft materials in clinically relevant, multi-endpoint animal models in determining spinal fusion efficacy.

REFERENCES

1. Dimitriou R, Mataliotakis GI, Angoules AG, et al. Complications following autologous bone graft harvesting from the iliac crest and using the RIA: a systematic review. *Injury.* 2011;42:S3–S15.
2. Kurien T, Pearson RG, Scammell BE. Bone graft substitutes currently available in orthopaedic practice: the evidence for their use. *Bone Joint J.* 2013;95-B:583–597.
3. Jones JR, Brauer DS, Hupa L, et al. Bioglass and bioactive glasses and their impact on healthcare. *Int J Appl Glas Sci.* 2016;7:423–434.
4. LeGeros RZ. Properties of osteoconductive biomaterials: calcium phosphates. *Clin Orthop Relat Res.* 2002;395:81–89.
5. Habibovic P, Yuan H, Van Der Valk CM, et al. 3D microenvironment as essential element for osteoinduction by biomaterials. *Biomaterials.* 2005;26:3565–3575.
6. Duan R, van Dijk LA, Barbieri D, et al. Accelerated bone formation by biphasic calcium phosphate with a novel sub-micron surface topography. *Eur Cell Mater.* 2019;37:60–73.
7. Habibovic P, Yuan H, van den Doel M, et al. Relevance of osteoinductive biomaterials in critical-sized orthotopic defect. *J Orthop Res.* 2006;24:867–876.
8. Yuan H, Fernandes H, Habibovic P, et al. Osteoinductive ceramics as a synthetic alternative to autologous bone grafting. *Proc Natl Acad Sci USA.* 2010;107:13614–13619.
9. Duan R, Barbieri D, Luo X, et al. Submicron-surface structured tricalcium phosphate ceramic enhances the bone regeneration in canine spine environment. *J Orthop Res.* 2016;34:1865–1873.
10. Xynos ID, Hukkanen MVJ, Batten JJ, et al. Bioglass ®45S5 stimulates osteoblast turnover and enhances bone formation in vitro: Implications and applications for bone tissue engineering. *Calcif Tissue Int.* 2000;67:321–329.
11. Xynos ID, Edgar AJ, Buttery LD, et al. Gene-expression profiling of human osteoblasts following treatment with the ionic products of Bioglass 45S5 dissolution. *J Biomed Mater Res.* 2001;55:151–157.
12. Qiu Z, Yang H, Wu J, et al. Ionic dissolution products of NovaBone® promote osteoblastic proliferation via influences on the cell cycle. *J Int Med Res.* 2009;37:737–745.
13. Andersson H, Kangasniemi I. Calcium phosphate formation at the surface of bioactive glass in vitro. *J Biomed Mater Res.* 1991;25:1019–1030.
14. Filgueiras MR, La Torre G, Hench LL. Solution effects on the surface reactions of a bioactive glass. *J Biomed Mater Res.* 1993;27:445–453.
15. Hench LL, Splinter RJ, Allen WC, et al. Bonding mechanisms at the interface of ceramic prosthetic materials. *J Biomed Mater Res.* 1971;5:117–141.
16. Hench LL. Bioceramics: from concept to clinic. *J Am Ceram Soc.* 1991;74:1487–1510.
17. van Dijk LA, Barbieri D, Barrere-de Groot F, et al. Efficacy of a synthetic calcium phosphate with submicron surface topography as autograft extender in lapine posterolateral spinal fusion. *J Biomed Mater Res B Appl Biomater.* 2019;107:2080–2090.

18. van Dijk LA, Duan R, Luo X, et al. Biphasic calcium phosphate with submicron surface topography in an Ovine model of instrumented posterolateral spinal fusion. JOR. *Spine*. 2018;1:e1039.

19. Boden SD, Schimandle JH, Hutton WC. An experimental lumbar intertransverse process spinal fusion model. Radiographic, histologic, and biomechanical healing characteristics. *Spine (Phila Pa 1976)*. 1995;20:412–420.

20. Lenke LG, Bridwell KH, Bullis D, et al. Results of in situ fusion for isthmic spondylolisthesis. *J Spinal Disord*. 1992;5:433–442.

21. Fedorov A, Beichel R, Kalpathy-Cramer J, et al. 3D slicer as an image computing platform for the quantitative imaging network. *Magn Reson Imaging*. 2012;30:1323–1341.

22. Zukic D, Vicory J, McCormick M, et al. N-D morphological contour interpolation. *Insight J*. 2016.

23. Mabud T, Norden J, Veeravagu A, et al. Complications, readmissions, and revisions for spine procedures performed by orthopedic surgeons versus neurosurgeons: a retrospective, longitudinal study. *Clin Spine Surg*. 2017;30:E1376–E1381.

24. Deyo RA, Martin BI, Kreuter W, et al. Revision surgery following operations for lumbar stenosis. *J Bone Joint Surg Am*. 2011;93: 1979–1986.

25. Martin BI, Mirza SK, Comstock BA, et al. Reoperation rates following lumbar spine surgery and the influence of spinal fusion procedures. *Spine (Phila Pa 1976)*. 2007;32:382–387.

26. Malter AD, McNeney B, Loeser JD, et al. 5-year reoperation rates after different types of lumbar spine surgery. *Spine (Phila Pa 1976)*. 1998;23:814–820.

27. Oonishi H, Kushitani S, Yakusawa E, et al. Particulate bioglass compared with hydroxyapatite as a bone graft substitute. *Clin Orthop Relat Res*. 1997;334:316–325.

28. Fujishiro Y, Hench LL, Oonishi H. Quantitative rates of in vivo bone generation for Bioglass® and hydroxyapatite particles as bone graft substitute. *J Mater Sci Mater Med*. 1997;8:649–652.

29. Oonishi H, Hench LL, Wilson J, et al. Quantitative comparison of bone growth behavior in granules of Bioglass®, A-W glass-ceramic, and hydroxyapatite. *J Biomed Mater Res*. 2000;51:37–46.

30. Wang Z, Lu B, Chen L, et al. Evaluation of an osteostimulative putty in the sheep spine. *J Mater Sci Mater Med*. 2011;22:185–191.

31. Wheeler DL, Stokes KE, Hoellrich RG, et al. Effect of bioactive glass particle size on osseous regeneration of cancellous defects. *J Biomed Mater Res*. 1998;41:527–533.

32. Walsh WR, Oliver RA, Christou C, et al. Critical size bone defect healing using collagen-calcium phosphate bone graft materials. *PLoS One*. 2017;12:e0168883.

33. Walsh WR, Vizesi F, Michael D, et al. β-TCP bone graft substitutes in a bilateral rabbit tibial defect model. *Biomaterials*. 2008;29: 266–271.

34. Elshahat A, Shermak MA, Inoue N, et al. The use of novabone and norian in cranioplasty: a comparative study. *J Craniofac Surg*. 2004;15:483–489.

35. Kanayama M, Cunningham BW, Setter TJC, et al. Does spinal instrumentation influence the healing process of posterolateral spinal fusion? An in vivo animal model. *Spine (Phila Pa 1976)*. 1999;24: 1058–1065.

36. Pearce AI, Richards RG, Milz S, et al. Animal models for implant biomaterial research in bone: a review. *Eur Cell Mater*. 2007;13:1–10.

37. Wilke HJ, Kettler A, Wenger KH, et al. Anatomy of the sheep spine and its comparison to the human spine. *Anat Rec*. 1997;247:542–555.

38. Wilke HJ, Kettler A, Claes LE. Are sheep spines a valid biomechanical model for human spines? *Spine (Phila Pa 1976)*. 1997;22:2365–2374.

39. Drespe IH, Polzhofer GK, Turner AS, et al. Animal models for spinal fusion. *Spine J*. 2005;5:S209–S216.

40. Wancket LM. Animal models for evaluation of bone implants and devices: comparative bone structure and common model uses. *Vet Pathol*. 2015;52:842–850.

41. Walsh WR, Loefler A, Nicklin S, et al. Spinal fusion using an autologous growth factor gel and a porous resorbable ceramic. *Eur Spine J*. 2004;13:359–366.

42. Kroeze RJ, van der Veen AJ, van Royen BJ, et al. Relation between radiological assessment and biomechanical stability of lumbar interbody fusion in a large animal model. *Eur Spine J*. 2013;22: 2731–2739.

43. Wang T, Ball JR, Pelletier MH, et al. Biomechanical evaluation of a biomimetic spinal construct. *J Exp Orthop*. 2014;1:3.

44. Heggeness MH, Esses SI. Classification of pseudarthroses of the lumbar spine. *Spine (Phila Pa 1976)*. 1991;16(suppl):S449–S454.

45. Aghi MK, Walcott BP, Nahed BV, et al. Determinants of initial bone graft volume loss in posterolateral lumbar fusion. *J Clin Neurosci*. 2011;18:1193–1196.

46. Ha KY, Lee JS, Kim KW. Bone graft volumetric changes and clinical outcomes after instrumented lumbar or lumbosacral fusion: A prospective cohort study with a five-year follow-up. *Spine (Phila Pa 1976)*. 2009;34:1663–1668.

47. Kim KW, Ha KY, Moon MS, et al. Volumetric change of the graft bone after intertransverse fusion. *Spine (Phila Pa 1976)*. 1999;24:428–433.

48. Duan R, Barbieri D, Luo X, et al. Variation of the bone forming ability with the physicochemical properties of calcium phosphate bone substitutes. *Biomater Sci*. 2018;6:136–145.

49. Zhang R, Liang Y, Wei S. M2 macrophages are closely associated with accelerated clavicle fracture healing in patients with traumatic brain injury: a retrospective cohort study. *J Orthop Surg Res*. 2018; 13:213.

50. Zheng ZW, Chen YH, Wu DY, et al. Development of an accurate and proactive immunomodulatory strategy to improve bone substitute material-mediated osteogenesis and angiogenesis. *Theranostics*. 2018;8:5482–5500.

51. Jamalpoor Z, Asgari A, Lashkari MH, et al. Modulation of macrophage polarization for bone tissue engineering applications. *Iran J Allergy Asthma Immunol*. 2018;17:398–408.

52. Barbieri D, Yuan H, Ismailoğlu AS, et al. Comparison of two moldable calcium phosphate-based bone graft materials in a noninstrumented canine interspinous implantation model. *Tissue Eng Part A*. 2017;23:1310–1320.

53. Hing KA, Wilson LF, Buckland T. Comparative performance of three ceramic bone graft substitutes. *Spine J*. 2007;7:475–490.

54. Gough JE, Notingher I, Hench LL. Osteoblast attachment and mineralized nodule formation on rough and smooth 45S5 bioactive glass monoliths. *J Biomed Mater Res A*. 2004;68:640–650.

55. Gough JE, Jones JR, Hench LL. Nodule formation and mineralisation of human primary osteoblasts cultured on a porous bioactive glass scaffold. *Biomaterials*. 2004;25:2039–2046.

56. Westhauser F, Karadjian M, Essers C, et al. Osteogenic differentiation of mesenchymal stem cells is enhanced in a 45S5-supplemented beta-TCP composite scaffold: an in-vitro comparison of Vitoss and Vitoss BA. *PLoS One*. 2019;14:e0212799.

57. Schmitt JM, Buck DC, Joh S-P, et al. Comparison of porous bone mineral and biologically active glass in critical-sized defects. *J Periodontol*. 1997;68:1043–1053.

58. Moreira-Gonzalez A, Lobocki C, Barakat K, et al. Evaluation of 45S5 bioactive glass combined as a bone substitute in the reconstruction of critical size calvarial defects in rabbits. *J Craniofac Surg*. 2005;16:63–70.

59. Kobayashi H, Turner AS, Seim HB, et al. Evaluation of a silica-containing bone graft substitute in a vertebral defect model. *J Biomed Mater Res A*. 2010;92:596–603.